Electronic Supplementary Material (ESI) for Journal of Materials Chemistry A

Supporting Information

Nickel oxide nanoflowers: formation, structure, magnetic property and adsorptive performance towards organic dyes and heavy metal ions

Le Xin Song*, Zheng Kun Yang, Yue Teng, Juan Xia and Pu Du

Department of Chemistry, University of Science and Technology of China, Jin Zhai Road 96, Hefei 230026, China

E-mail: solexin@ustc.edu.cn; Fax: +86-551-63601592; Tel: +86-551-63492002

Experimental Section

***Materials*:** Nickel chloride hydrates ($NiCl_2·6H_2O$) was obtained from Sinopharm Chemical Reagent Company. Sodium tartrate hydrates ($Na_2C_4H_4O_6·2H_2O$) and a commercial nickel oxide (NiO) were purchased from Shanghai Chemical Reagent Company. Congo red, methyl orange and methylene blue were from Aladdin Chemistry Co. Ltd. Lead nitrate $Pb(NO_3)_2$ and mercuric chloride ($HgCl_2$) were purchased from Shanghai Chemical Reagent Company and used as received without further purification.

***Preparation of the NEG precursor and NiO nanoflowers*:** The NEG nanoflowers were synthesized by a facile hydrothermal process: 0.119 g (0.5 mmol) of six hydrates of $NiCl_2$ and 0.23 g (1 mmol) of two hydrates of ST were dissolved in 40 mL deionized water at room temperature, stirring for 30 minutes. Then, the solution was transferred into a Teflon-lined stainless steel autoclave (50 mL), sealed, and heated at 473 K for 24 h. A light green crystal product (NEG) was collected *via* centrifugation at 9000 rpm for 10 min, and further washed with distilled water and finally with ethanol several times, and dried in vacuum at 333 K for 12 h. The NiO nanoflowers were prepared by thermal decomposition of the as-obtained NEG at 673 K in a muffle furnace. After 1.5 h heating, the furnace was gradually cooled to room temperature, producing a gray NiO material.

***Materials characterization*:** XRD measurements were recorded on a Philips X'Pert Pro X-ray diffractometer using a monochromatized Cu Kα radiation source (40 kV, 40 mA) with a wavelength of 0.1542 nm and analyzed in the range $10° \leq 2\theta \leq 70°$. FE-SEM images were obtained on a Supra 40 operated at 5 kV. TEM (HR-TEM) images and selected area electron diffraction (SAED) patterns were obtained with a JEF 2100F field-emission transmission electron microscope using an accelerating voltage of 200 kV. XPS analysis was done using an ESCALAB250 spectrometer, with Al Kα excitation radiation (1486.6 eV) in ultra-high vacuum conditions (2.00×10^{-9} Torr). Thermal gravimetric (TG) measurements were recorded on a ShimadzuTGA-50 thermal gravimetric analyzer at a constant heating rate of 10.0 $K·min^{-1}$ under air atmosphere with a gas flow of 25 $mL·min^{-1}$. Fourier transform infrared (FTIR) spectra were obtained with a Bruker Equinox 55 spectrometer in KBr pellets. Raman spectrum was collected at room temperature with a LABRAM-HR Confocal Laser MicroRaman spectrometer in the range 300–750 cm^{-1}. Magnetic measurements were performed in a Quantum Design (San Diego, USA) Magnetic Properties Measurement System (MPMS-7XL) equipped with a SQUID by a vibrating sample magnetometer. UV-vis spectra were carried out on a Shimadzu UV 2401-(PC) spectrometer in the range 190–700 nm. The pH values of solution were measured using Leici PHSJ-3F laboratory pH-meter (Leici Instrument Factory, Shanghai, China).

***Removal of CR*:** Different amounts (0–0.5 $g·L^{-1}$) of the NiO nanoflowers were added to a group of aqueous solutions of CR with the same concentration of 100 $mg·L^{-1}$ and the solutions were thoroughly mixed under vigorous stirring for 3 h. Subsequently, the solid was separated by centrifugation (12000 rpm) and the supernatant solutions were analysed with UV-vis spectroscopy. The concentrations of CR in the solutions were determined using a linear calibration curve over 5−80 $mg·L^{-1}$ based on the absorbance values at 495 nm. To estimate the q_e values, the C_0 values of CR were varied in the range of 100–500 $mg·L^{-1}$, and the dosage of the NiO nanoflowers was kept at 0.5 $g·L^{-1}$.

***Removal of heavy metal ions*:** A series of solutions containing different concentrations of Pb^{2+} and Hg^{2+} (6.25, 12.5, 31.25, 62.5, 125, 312.5 $mg·L^{-1}$) was prepared using $Pb(NO_3)_2$ and $HgCl_2$ as the sources of heavy metal ions, respectively. To obtain the adsorption isotherms, 5 mg of the NiO nanoflower was added into 10 mL of the above solutions at room temperature. After stirring for 3 h, the solid was separated by centrifugation (12000 rpm) and the supernatant solutions were analysed using inductively coupled plasma-optical emission spectroscopy (Optima 7300DV) to determine the concentration of the remaining metal ions.

Figure S1 shows that the decomposition of the NEG nanoflowers divided in two stages: (i) a slight mass loss of 3.56% (crystal water release) and (ii) a sharp mass loss of 36.93% due to the decomposition of NEG to produce NiO corresponding tothe release (37.08%) of CO_2 and H_2O (see Equation 1).

$$2NiC_2H_4O_2 + 5O_2 \xrightarrow{\triangle} 2NiO + 4CO_2 + 4H_2O \qquad 1)$$

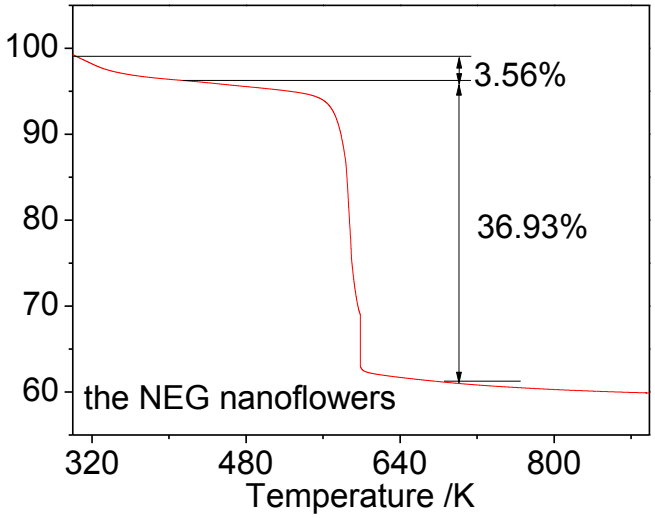

Figure S1. TG curve of the NEG nanoflowers

Figure S2 indicates the FTIR spectrum of the NEG nanoflowers, the O–H stretching vibration band appears at 3481 cm^{-1}, and the Ni−O stretching vibration band remains at 647 cm^{-1}. The peaks at 2957 and 2908 cm^{-1} are attributed to the stretching vibration band of CH_2. No C=O stretching vibration band was detected.

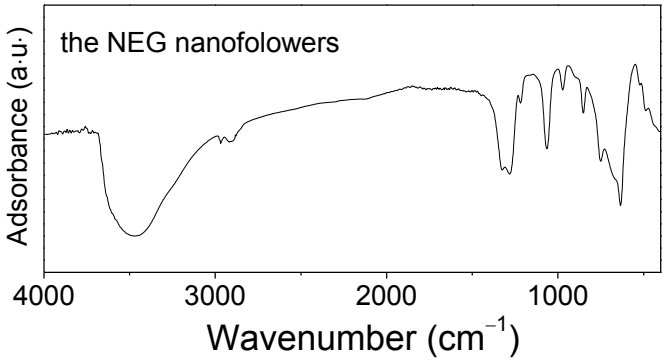

Figure S2. FTIR spectrum of the NiO nanoflowers.

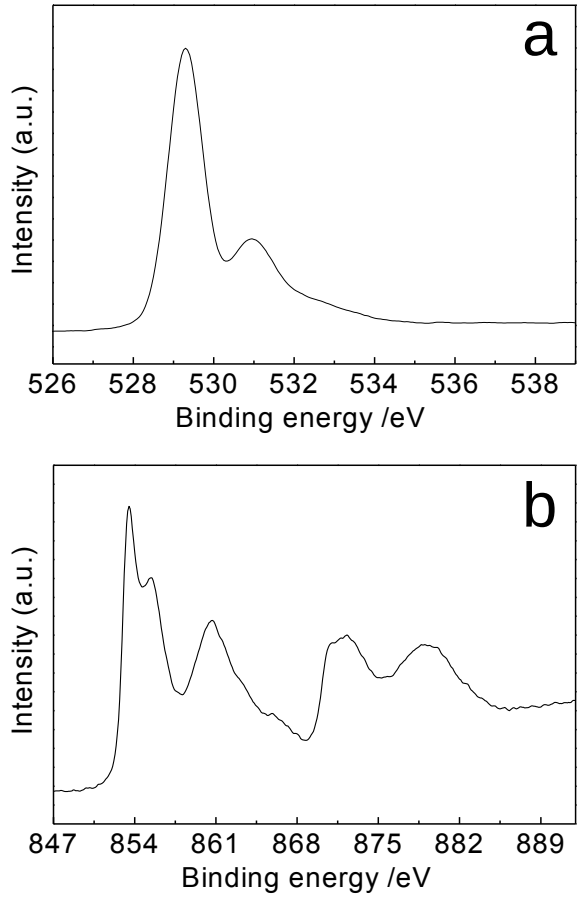

Figure S3. XPS spectra of NiO: (a) O_{1s} and (b) Ni_{2p}.

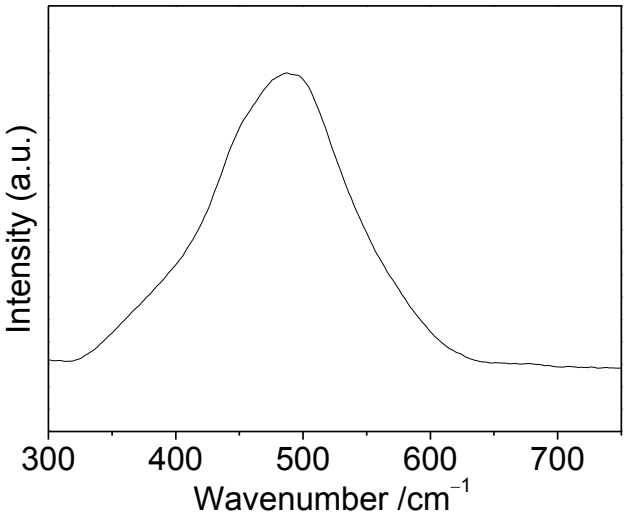

Figure S4. The Raman spectrum of the NiO nanoflowers.

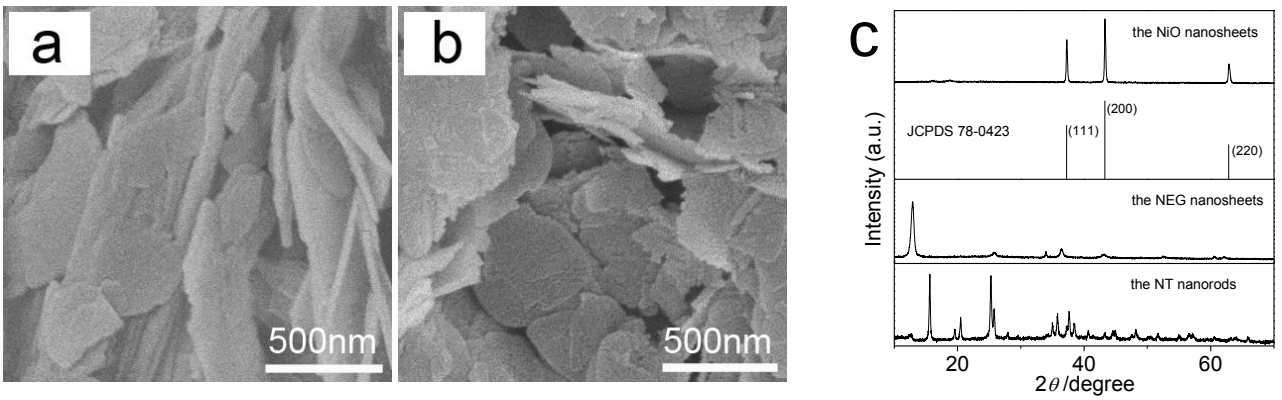

Figure S5. FE-SEM images of (a) the NEG nanosheets and (b) the NiO nanosheets and the XRD patterns of NT nanorods, the NEG nanosheets and the NiO nanosheets (c).

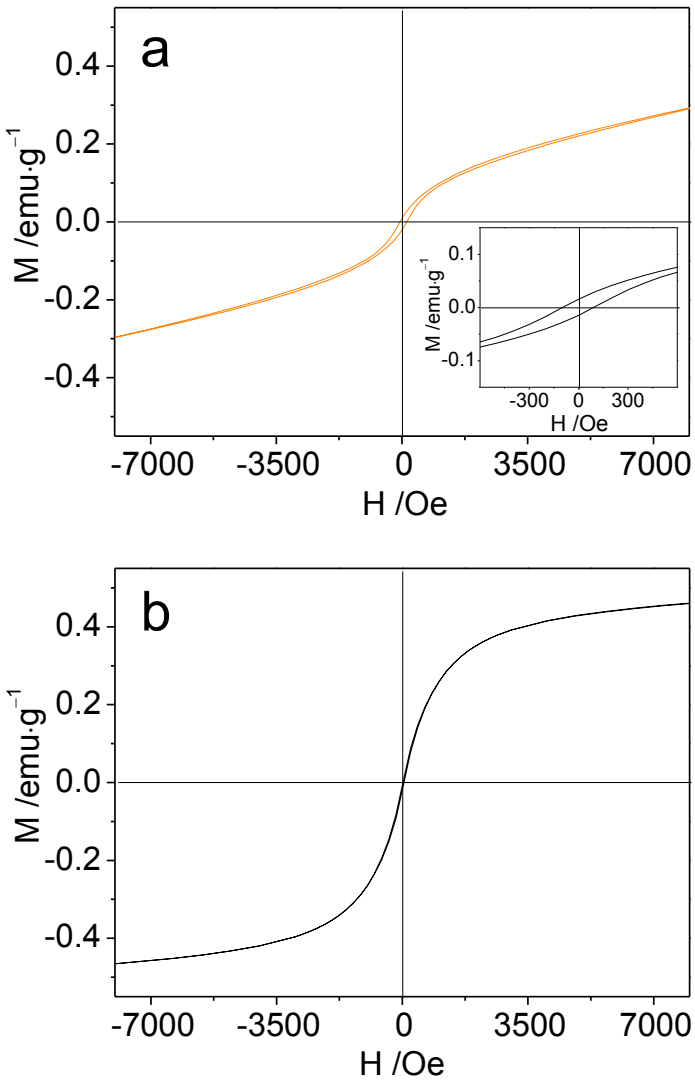

Figure S6. Field (*H*) dependence of magnetization (*M*) of (a) the NiO nanoflowers (the inset is the enlargement of the *M*–*H* at lower magnetic fields) and (b) the NiO nanosheets at 300 K.

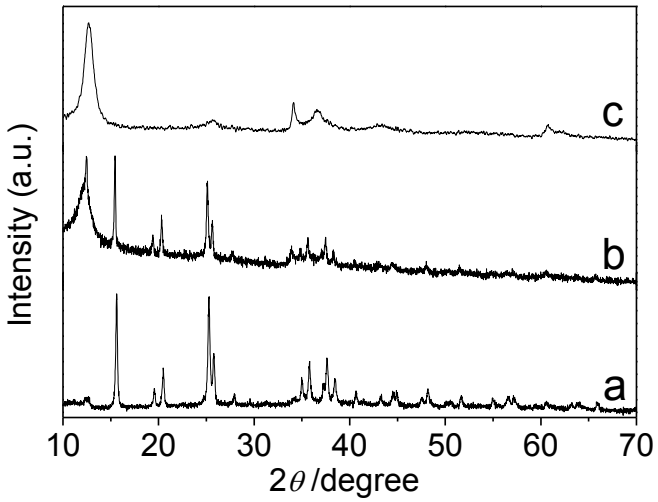

Figure S7. XRD patterns of (a) the NT nanorods, (b) the mixture of NT nanorods and NEG nanoflowers, and (c) the NEG nanoflowers.

Figure S8 illustrates the TG profile of the NT nanorods. The mass loss of 63.79% in the anhydrous NT curve corresponds to the release (63.86%) of CO_2 and H_2O in the decomposition of the NT to generate NiO (see Equation 2).

$$2NiC_4H_4O_6 + 5O_2 \xrightarrow{\triangle} 2NiO + 8CO_2 + 4H_2O \qquad 2)$$

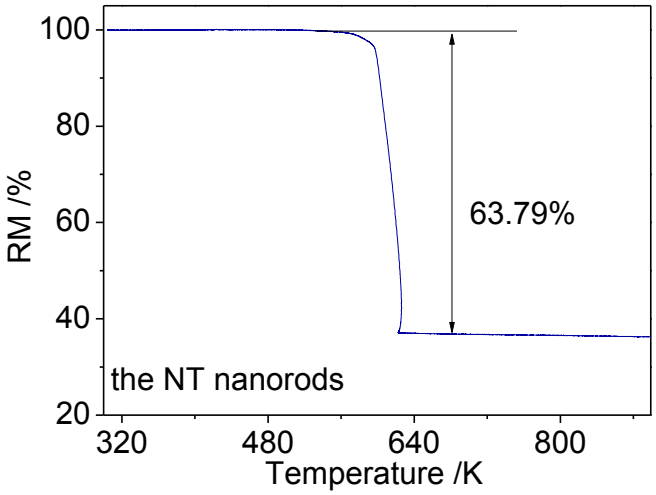

Figure S8. TG curve of the NT nanorods.

Figure S9 indicates the FTIR spectrum of the NT nanorods. In the FTIR spectrum of the NT nanorods, the O–H stretching vibration band, O–H bending band at and Ni−O stretching vibration band appear at 3394, 1416 and 647 cm^{-1}, respectively. In addition, we observed the strong C=O stretching vibration band at 1662 cm^{-1} and the C−C stretching vibration band at 1097 and 1017 cm^{-1}.

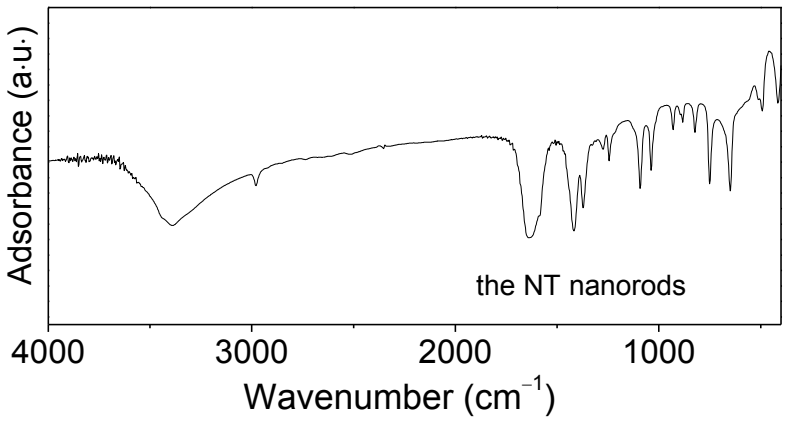

Figure S9. FTIR spectrum of the NT nanorods.

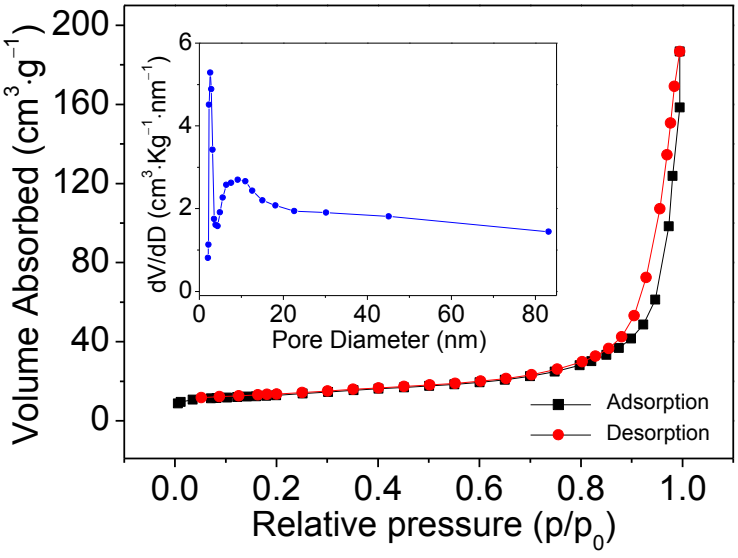

Figure S10. N_2 adsorption-desorption isotherm and pore size distribution curve of the NiO nanoflowers.

Table S1. pH values of the CR solution on the NiO nanoflowers during adsorption.

CR initial concentration /mg·g^{-1}	pH					
	0 h	0.5 h	1.5 h	3 h	4 h	5 h
50	6.98	6.94	6.95	7.15	7.15	7.15
100	6.61	6.89	7.01	7.11	7.11	7.11
200	6.43	6.89	6.98	7.08	7.08	7.08
300	6.41	6.82	6.92	6.96	6.96	6.96
400	6.33	6.54	6.72	6.84	6.84	6.84
500	6.19	6.31	6.45	6.56	6.56	6.56

Table S2. pH values of the Pb^{2+} solution on the NiO nanoflowers during adsorption.

Pb^{2+} initial concentration /mg·g^{-1}	pH					
	0 h	0.5 h	1.5 h	3h	4 h	5 h
6.25	6.53	7.12	7.21	7.28	7.28	7.29
12.5	5.80	6.73	6.98	7.25	7.25	7.25
31.25	5.15	5.89	6.19	6.25	6.25	6.24
62.5	4.35	4.93	5.21	5.33	5.34	5.34
125	4.18	4.67	4.72	4.85	4.85	4.85
312.5	4.01	4.12	4.34	4.44	4.44	4.45

Table S3. pH values of the Hg^{2+} solution on the NiO nanoflowers during adsorption.

Hg^{2+} initial concentration /mg·g^{-1}	pH					
	0 h	0.5 h	1.5 h	3 h	4 h	5 h
6.25	5.02	5.59	5.71	6.37	6.37	6.38
12.5	4.89	5.13	5.34	5.97	5.98	5.97
31.25	4.69	4.98	5.56	5.96	5.96	5.96
62.5	4.62	4.99	5.10	5.66	5.68	5.68
125	4.59	4.89	5.10	5.56	5.56	5.57
312.5	4.59	4.89	5.01	5.32	5.32	5.32

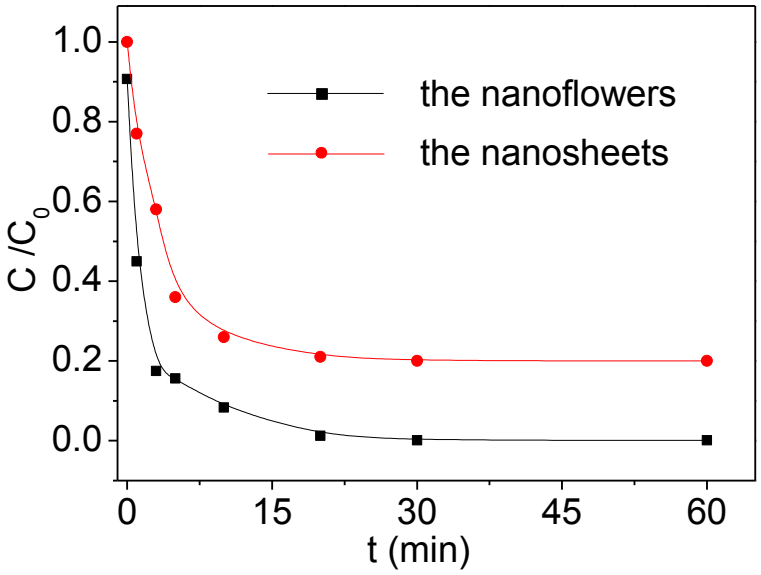

Figure S11. Adsorption rate of CR on the NiO nanoflowers and NiO nanosheets.

Table S4. The q_m values of several materials for CR.

adsorbents	references	q_m /mg·g^{-1}	testing parameters			
			adsorbent dosage /g·L^{-1}	adsorbate concentration /mg·L^{-1}	contact time /h	temperature /K
NiO nanoflowers	this study	525	0.5	50~500	3	298
NiO nanosheets	this study	180	0.5	50~500	3	298
the commercial NiO	this study	28	0.5	50~500	3	298
NiO nanosheets	[30]	35.15	2.5	100	6	298
hierarchical NiO nanosheets	[31]	151.7	0.2	15~50	7.5	298
α-FeOOH hollow spheres	[32]	275	0.5	100~500	3	298
mesoporous Fe_2O_3	[33]	53	1.25	100	1	298
CeO_2 hollow spheres	[34]	84	0.75	50	2	298
MnO_2 hollow microspheres	[35]	60	1.5	100	0.5	298

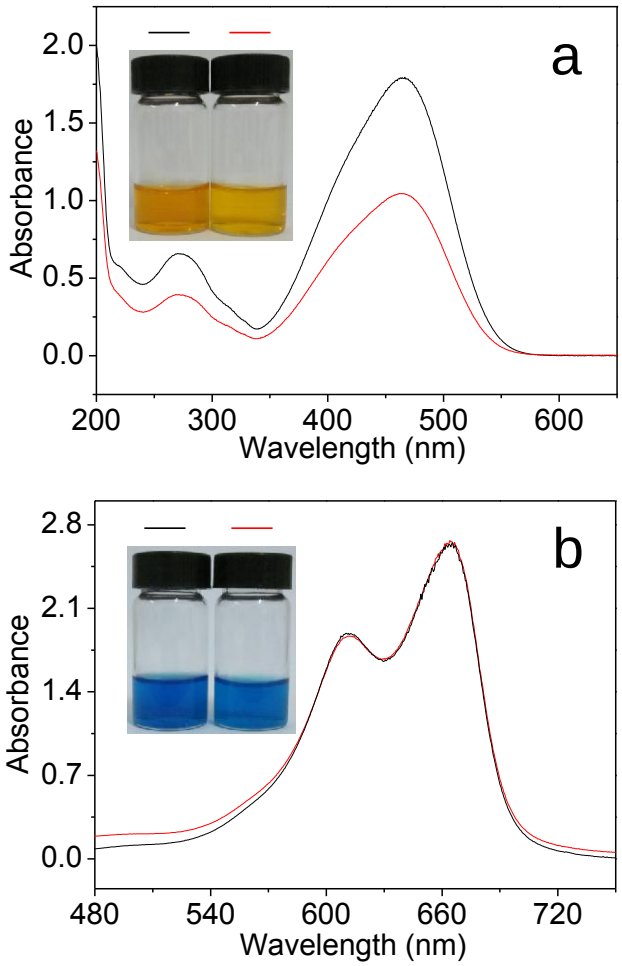

Figure S12. UV-vis absorption spectra and digital images of the organic dyes (20 mg·L^{-1}) before (black curve) and after (red curve) treated with the NiO nanoflowers (0.5 g·L^{-1}): (a) methyl orange, (b) methylene blue.

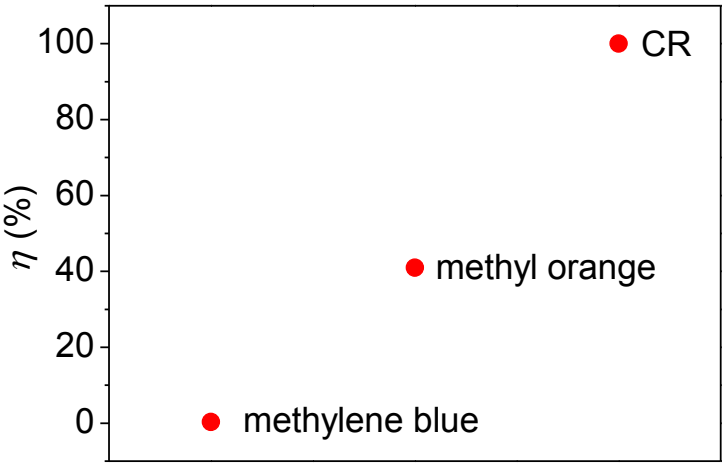

Figure S13. η values of different organic dyes at the same initial concentration 20 mg·L^{-1} onto the NiO nanoflowers (0.5 g·L^{-1}).

Table S5. The q_m values of several materials for Pb^{2+}.

adsorbents	references	q_m /mg·g^{-1}	testing parameters			
			adsorbent dosage /g·L^{-1}	adsorbate concentration /mg·L^{-1}	contact time /h	temperature /K
NiO nanoflowers	this study	125	0.5	6.25~312.5	3	298
NiO nanosheets	this study	108	0.5	6.25~312.5	3	298
the commercial NiO	this study	13.6	0.5	6.25~312.5	3	298
α-FeOOH hollow spheres	[32]	80	0.5	10~1500	3	298
α-FeOOH microspheres	[36]	103	0.5	10~1000	3	298
magnesium silicate hollow spheres	[37]	65	5	106.42	2	298
Fe_2O_3 hollow spindles	[38]	5.3	1	16.39	2	298

Table S6. The q_m values of several materials for Hg^{2+}.

adsorbents	references	q_m /mg·g^{-1}	testing parameters			
			adsorbent dosage /g·L^{-1}	adsorbate concentration /mg·L^{-1}	contact time /h	temperature /K
NiO nanoflowers	this study	84	0.5	6.25~312.5	3	298
NiO nanosheets	this study	45	0.5	6.25~312.5	3	298
the commercial NiO	this study	8.7	0.5	6.25~312.5	3	298
silicon hollow microsphere sensor	[39]	32.3	3	0.20~2006	1	298